PERGAMON International Journal of Impact Engineering 25 (2001) 819–829

INTERNATIONAL JOURNAL OF IMPACT ENGINEERING

www.elsevier.com/locate/ijimpeng

Analysis of ceramic/metal armour systems

M. Lee[a,*], Y.H. Yoo[b]

[a] *Department of Mechanical Engineering, Sejong University, Seoul 143-747, South Korea*
[b] *Agency for Defense Development, Taejon, South Korea*

Received 26 February 2001; received in revised form 25 May 2001

Abstract

A combined numerical and experimental study for the analysis of ceramic/metal composite armour system against 40.7 g steel projectiles has been performed. The ballistic performance of the add-on lightweight armours was examined by varying the thickness of tiles, while maintaining equal areal density of the system. A numerical study using smoothed particle hydrodynamics scheme is promising since the major distinguishing features of composite armour systems such as, projectile erosion, crack propagation, ceramic conoid formation and failure of backing plate, are successfully captured. Simulation results for ballistic limits appear to match fairly well with the test values and reveal an optimum value of the front plate to back plate thickness ratio.

Keywords: Armour; Areal density; Ballistic limit; Smoothed particle hydrodynamics (SPH)

1. Introduction

There has been substantial interest recently in studies of ceramic materials backed by a ductile metal plate against small and medium caliber projectiles [1,2]. It is well known that the backup metal, which delays the initiation of tensile failure in the ceramic initiating at the ceramic/backing plate interface and allows more projectile erosion, enhances the ballistic performance of add-on armour systems [3]. Another role of the backing metal is the absorption of kinetic energy of ceramic fragments. The complexity of the system analysis lies in the fact that different deformation and failure mechanisms contributing to target perforation occur at different stages of the penetration process. Besides many parameters for each material description, the front plate to back plate thickness ratio and impact velocity can also govern the penetration process. Hence, the

*Corresponding author. School of Mechanical and Aerospace Engineering, Sejong University, 98 Kwangjin-Gu, Kunja-Dong, Seoul 143-737, South Korea. Tel.: +82-2-3408-3282; fax: +82-2-3408-3333.
E-mail address: mlee@sejong.ac.kr (M. Lee).

0734-743X/01/$ - see front matter
PII: S0734-743X(01)00025-2

design of composite armour systems based on the understanding of real impact events is really a challenging subject and deserves a sophisticated research work.

Although experimental approach offers most accurate results, it is expensive and sometimes does not provide detail information of the impact event. Another way to analyze the detailed penetration process is to use computer predictions. Until now, simulation has not provided satisfying results for the composite armour system. Due to the complexity of material parameters, description of various aspects of the interaction between the projectile and the add-on composite armour target requires advanced material and failure models. Once the material strength and failure models are verified, however, it can be easily extended to more real situations, such as oblique impact and multiple composite layers.

In the current study, several fire tests were conducted and the data were used for verification of the numerical approach. In the simulations, the cumulative damage model [4] with smoothed particle hydrodynamics (SPH) scheme [5] was used. The major features of composite armour systems such as, projectile erosion, crack propagation, ceramic conoid formation and failure of the back plate are successfully identified. We present the results of the impact of 40.7 g steel projectiles on ceramic/metal composite armours. A study conducted by Hetherington [6] examined the optimization of two component composite armours against 7.62 mm ammunition. Simulation results for selected target configurations revealed that there exists an optimum thickness ratio of two layers, which are maintained at equal areal density.

2. Experiments

Armours of alumina backed by aluminum against hard steel projectiles are designed to determine the ballistic limit velocity, V_{50}, below which the projectile fails to perforate the armour system. This is because the determination of ballistic limit is of importance in the design of armour systems. The steel (7850 kg/m^3) projectile has a dimension of 52.5 mm overall length and 12.5 mm diameter. It has a mass of approximately 40.7 g, and yield strength is 2.3 GPa. Alumina (3380 kg/m^3) was used as a front plate material. The Vickers hardness is 8.8 GPa. 5083 aluminum (2260 kg/m^3) was chosen as a back plate. The front plate to back plate thickness ratio (h_1/h_2) is varied, while maintaining equal areal density. The maximum thickness of ceramic and metal plate is 25 and 25.4 mm, respectively.

Based on the probabilistic technique using a substantial base of data, a series of impact experiments was conducted by changing the impact velocity until the ballistic limit is determined. In the experiment, the error is within 10 m/s. Table 1 displays the ballistic limit

Table 1
Experimental data for ballistic limits at equal areal density

Configuration	Alumina/aluminum thickness ratio (h_1/h_2)	Normalized V_{50}
C-1	0.39	1.0
C-2	0.79	1.036
C-3	1.65	1.097
C-4	3.95	1.009

velocities determined experimentally. The C-3 configuration shows the best ballistic efficiency. That is, the test data reveal that there exists an optimum thickness ratio in the composite armour systems.

3. Numerical simulations

3.1. Numerical schemes

Although Eulerian scheme has been used to simulate material responses involving large deformations, it introduces an inaccuracy associated with advection calculation. On the other hand, Lagangian scheme requires an artificial technique to treat large deformation event, even if it is more accurate to calculate the material interface. There exists a relatively new numerical technique compared with grid based Lagrangian and Eulerian techniques, which is SPH. SPH is a gridless technique for solving computational continuum dynamics problems and has some potential advantages over the grid based two schemes. Since SPH does not require a numerical grid, there is no grid-tangling problem for large deformation problems. Furthermore, the Lagrangian based technique allows efficient tracking of material deformation and history dependent behavior.

Impact into the lightweight armour plates involves several events, such as ceramic fracture, formation of ceramic conoid, tensile failure of a backing plate, and plugging, which are taking place at different stages of the penetration process. SPH scheme seems to be efficient in simulating such a complex problem. Especially, this scheme has been successfully applied to simulation of fracture phenomena. Hence, SPH scheme that has been implemented into AUTODYN hydrocode is used in this study.

3.2. Constitutive equations

There have been some efforts directed to develop constitutive models for brittle materials subjected to high strain rate and high pressures. Based on the observation that these materials experience little ductility and the strength is highly dependent on the pressure, the Mohr–Coulomb (MC) strength model and linear equation of state (EOS) are used in the current study. Since compressive strength usually increases with increased hydrostatic pressure, yield stress is modeled by a piecewise linear variation with pressure. The micromechanical failure of ceramic is modeled using a cumulative damage model [4].

To model the progressive crushing and subsequent weakening of ceramic material, a damage factor D, which is usually related to the amount of material straining, is introduced. The damage factor ranges from zero to $D_{\max}$ with zero indicating no damage and $D_{\max}$ representing complete damage. Damage is represented as a time dependent scalar. When the effective plastic strain reaches ε_{p1} the damage parameter D increases linearly with effective plastic strain up to a maximum value $D_{\max}$, as shown in Fig. 1.

$$D = D_{\max}\left(\frac{\varepsilon_p - \varepsilon_{p1}}{\varepsilon_{p2} - \varepsilon_{p1}}\right). \tag{1}$$

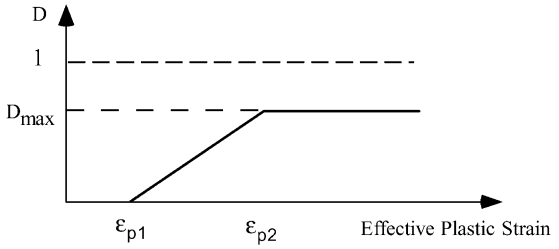

Fig. 1. Damage factor as a function of effective plastic strain.

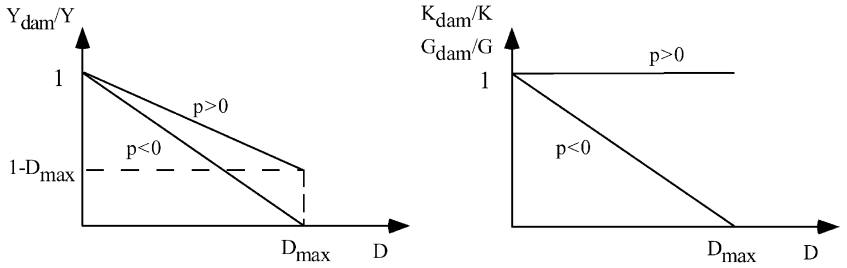

Fig. 2. Yield strength and elastic modulus as a function of damage factor.

In this approach, material softening is implemented by using the current value of the damage factor D through the modification of the bulk modulus, shear modulus and yield strength. If the hydrostatic pressure is positive, $Y_{\text{dam}} = Y(1 - D)$ and if the hydrostatic pressure is negative, $Y_{\text{dam}} = Y(1 - D/D_{\max})$. Note that fully damaged material ($D_{\max} = 0.7$) has some residual strength in compression but none in tension. The bulk modulus and shear modulus are unaffected in compression, while in tension they are progressively reduced to zero when damage is complete. These are illustrated graphically in Fig. 2.

The constitutive response for hard steel projectile was represented by the Johnson–Cook (JC) fracture model [7].

$$\sigma = 1.5\left[1 + 0.51(\varepsilon^p)^{0.26}\right][1 + 0.014\ln\dot{\varepsilon}^*]\left[1 - T^{*1.03}\right] \text{ GPa}, \tag{2}$$

where σ is the von Mises effective flow stress, ε^p the equivalent plastic strain, $\dot{\varepsilon}^*$ the dimensionless plastic strain rate, and the homogeneous temperature [8]. Aluminum plate is represented by piecewise linear strength model. That is, the von Mises effective flow stress is represented by a piecewise linear function of yield strength Y versus effective plastic strain. The maximum yield strength and ultimate strain were 0.45 and 0.25 GPa, respectively. The strain rate dependence and thermal softening expressions remain the same as in the JC model.

3.3. Modeling

Two-dimensional axisymmetry calculations were conducted. A particle size of 0.8 mm was used and resulted in ten SPH particles being placed inside a steel projectile in the radial direction. 461 particles were used in modeling the projectile. We used the same resolution in the ceramic and

backup plates. The range of total number of particles included in the simulation varied from 6311 to 7061, depending on the thickness ratios. Velocities on the outside boundary of the plates are fixed. The calculation usually took 100 min on a 600 MHz personal computer. A series of simulations was performed until the ballistic limit velocity was determined for each target configuration. The error is within 10 m/s.

3.4. Simulation results

Fig. 3 shows the simulated penetration processes of the C-1 configuration by a hard steel projectile. The impact velocity is 750 m/s. For this configuration of a relatively thin ceramic tile, no distinct formation of conoid is visible during the initial compressive phase. As shown in the figure, the ceramic tile is fully eroded by the projectile. As the projectile moves into the backing plate, it starts to behave as a rigid body. The second stage of penetration is the onset of shearing of a plug from the backing plate. Due to large strains occurring around the periphery of the projectile and tensile stresses developed by stretching the circular region on the back surface, fracture occurs and causes a plug to be detached in front of the projectile. The force the projectile exerts on the target is distributed over a relatively small circular area of the metal plate, so that no significant bending of the backing plate is observed. In this configuration, the projectile can fully erode thin ceramic tile with experiencing less deceleration, such that it can defeat the backing plate by perforation. The residual velocity is 240 m/s.

The simulated penetration processes of the C-2 configuration by a hard-steel projectile are shown in Fig. 4. The impact and residual velocities are 825 and 156 m/s, respectively. The major aspects of the interaction are almost the same as those shown in C-1 configuration, except ceramic still separating the projectile from the backing plate. The backing plate is defeated by perforation, rather than bulged and necked to failure by ductile failure.

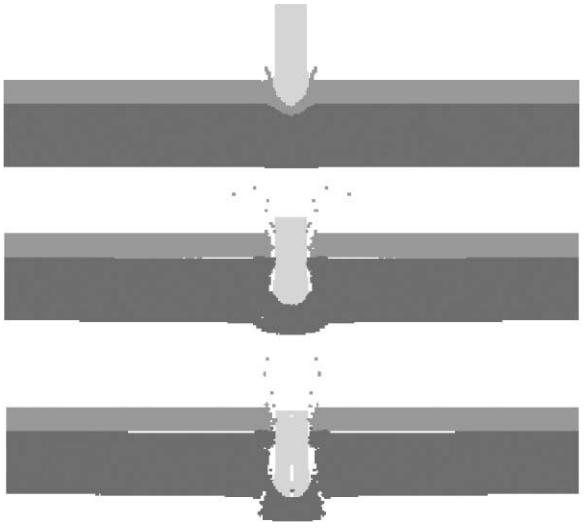

Fig. 3. Computations for configuration C-1, impact velocity 750 m/s.

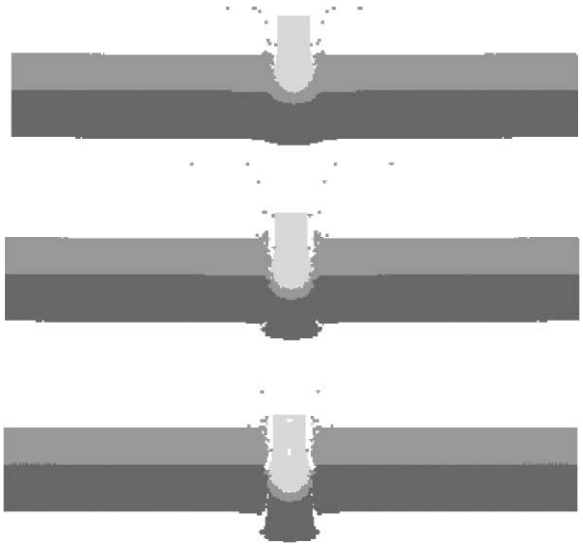

Fig. 4. Computations for configuration C-2, impact velocity 825 m/s.

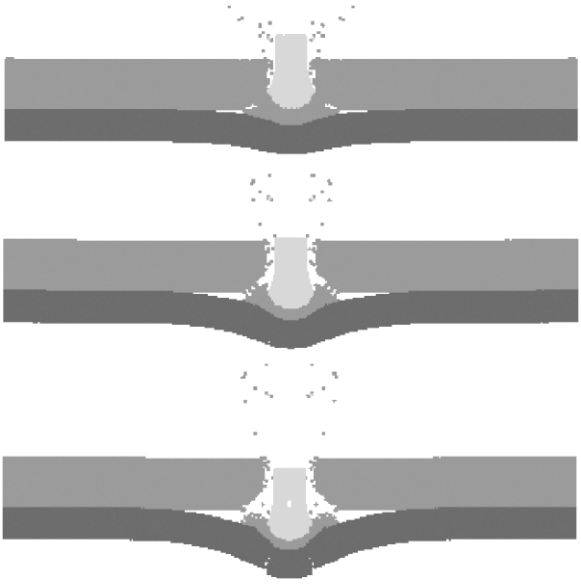

Fig. 5. Computations for configuration C-3, impact velocity 950 m/s.

Fig. 5 displays the simulated penetration processes of the C-3 configuration by a hard steel projectile. The impact velocity is 950 m/s. Conical cracks produce a volume of fragmented ceramic of a distinct conoid shape. The projectile experiencing erosion continues penetration into the volume of damaged ceramic. Due to the conoid located between the projectile and the backing plate, momentum can be distributed on the wide area of the backing plate. In this case, a

continuous bulging and a significant bending of the backing plate are observed. It can be conclude that a projectile experiences rapid deceleration due to the continuous interaction with a ceramic conoid backed by a metal plate of moderate backing thickness.

The simulated penetration processes of the C-4 configuration by a hard steel projectile at the impact velocity of 900m/s are shown in Fig. 6. In this configuration, a significant bending of the backing plate is observed. The cone shaped zone of damage simulated by Wilkins [3] is similar to calculated fracture conoid in this study. For this configuration of a thin backing plate, however, the resisting force provided by the backing plate is mainly due to dishing deformation. Due to small resistance, the projectile and the conoid can move as rigid bodies without experiencing significant deformation until full perforation. Although the literature often correlates petaling with thin plates, a plug, which is often correlated to thick plates, is observed in this configuration. This is due to hinges for dishing of the backing plate.

The history of projectile velocity is shown in Fig. 7 for two different configurations, C-1 and C-3. In general, the initial phase of penetration is the steady-state phase in which the projectile velocity remains constant at the initial impact velocity. During the deceleration phase that occurs after the steady-state phase, two slopes are identified for each curve. The rate of projectile deceleration is larger in the ceramic medium than in the aluminum medium. When we compare two curves from the figure, it can be seen that the deceleration rate in the C-3 configuration is larger than that in the C-1 configuration. Furthermore, the period of deceleration is also longer. This is attributed to the relatively thick ceramic tile, such that the ceramic in the C-3 configuration is held in place most rigidly by the backup plate.

In Fig. 8, residual projectile velocities determined numerically are given for different target configurations as a function of striking velocity. It can be seen that the C-3 configuration shows the best ballistic performance. For configuration C-3 and C-4 cases, the residual velocity starts to decrease around impact velocity of 950 m/s. This seems to be attributed to different deformation mechanisms operating at different stages of the process. In order to identify this trend, however, it

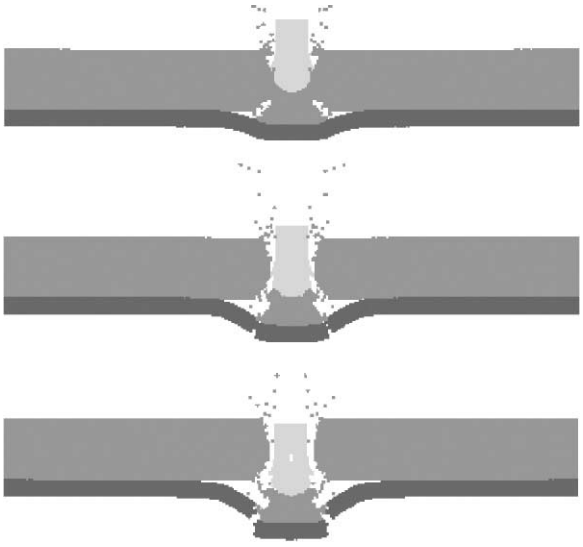

Fig. 6. Computations for configuration C-4, impact velocity 900 m/s.

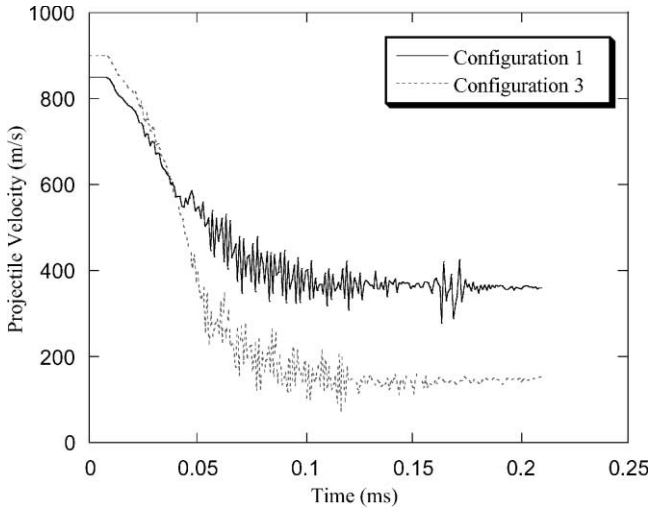

Fig. 7. Simulated projectile tail velocities for configurations, C-1 and C-3.

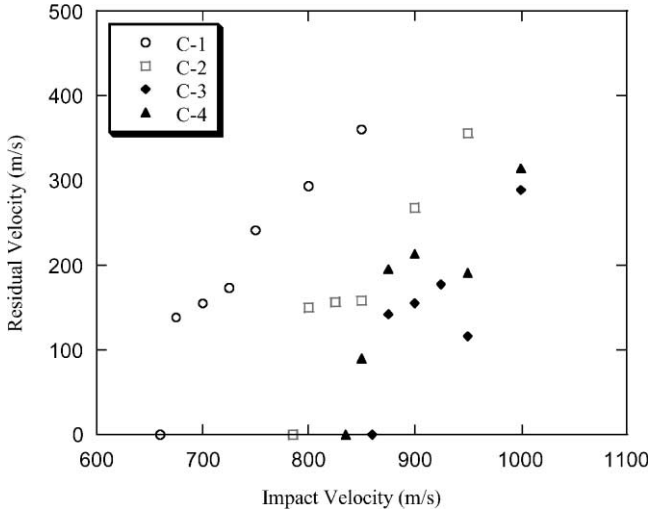

Fig. 8. Simulated residual velocities for different configurations of equal areal density.

is necessary to carry out further controlled simulations. Fig. 9 shows the normalized residual length of hard steel projectiles after perforation of ceramic/metal composite targets at normal incidence. The value of residual length displayed in the figure is an average one for different impact velocities.

4. Comparison of simulation and experiment

Fig. 10 shows the minimum perforation velocities (ballistic limit, V_{50}) determined experimentally (circles) and numerically (squares) for 40.7 g hard steel projectiles striking onto different

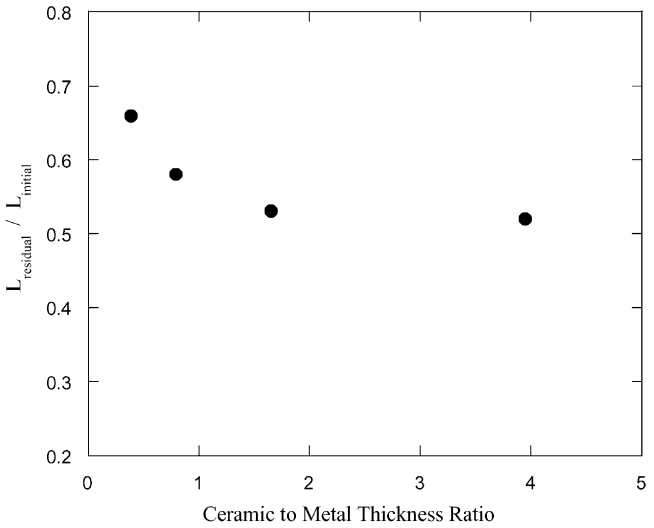

Fig. 9. Simulated residual lengths for different targets of equal areal density, the maximum variation with impact velocity was 0.6 mm.

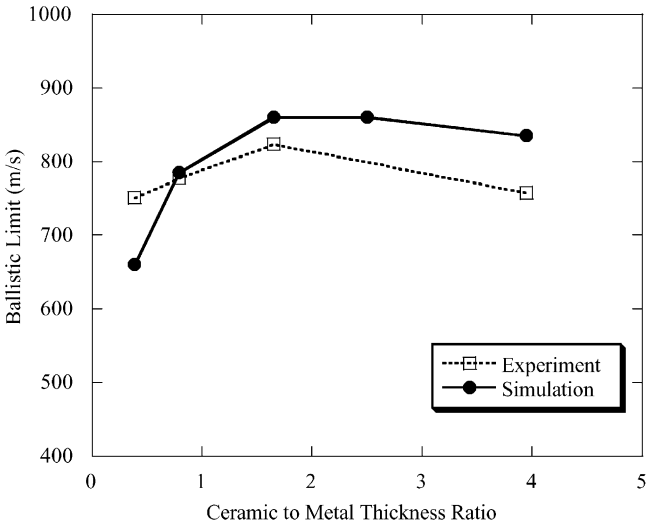

Fig. 10. Comparison of the ballistic limit velocities obtained numerically and experimentally for steel projectiles striking several configurations of equal areal density.

target configurations. In this analysis, $D_{\max} = 0.7$ at $\varepsilon_{p2} = 0.25$ and $D = 0$ at $\varepsilon_{p1} = 0.01$. It is shown that the results obtained from the present simulation match fairly well with the experimental ones. In the experiment, configuration C-4, which has the thinnest backing plate, and configuration C-1, which has the thickest backing plate, shows relatively the worst ballistic efficiency. In the simulation, however, the worst ballistic performance is observed in the C-1 configuration. Small discrepancy on the absolute value of the ballistic limits between experiment

and simulation can be attributed to both the experimental error and the material properties used in the simulation. Nevertheless, both solutions predict the same trend, showing the optimum composite thickness ratio in the region of 2.5.

Even for the penetration of 7.62 AP (armour piercing) round into alumina/aluminum composite armours, as shown in Fig. 11, the agreement is quite good. The theoretical and experimental data was given by Hetherington [6]. It is important to note that for values of h_1/h_2 between 1.5 and 3 ballistic performance of two component composite armours shows no significant difference. This is true of both ammunitions.

5. Discussion

The conoid volume and thickness separated from a backing plate and a projectile is dependent on different impact parameters, especially ceramic and metal plate thickness and impact velocity [9]. In many cases the conoid has a semiangle much lower than those assumed in the analytical models, so that conical crack formation is not limited to angles between 60° and 65°. In this study, the C-3 configuration leads to higher values of the ceramic conoid semiangle than the C-4 configuration does, although the impact velocity is slightly different. Furthermore, prediction of the conoid base diameter using the initial ceramic thickness is somewhat an overestimation since the projectile tip meets the cracking front near the center of ceramic medium. For relatively thin ceramic tiles, as shown in Figs. 3 and 4, a distinct conoid of wide base area is not visible. In this case, the penetration velocity is much higher and the damage in the composite armour is more localized around the impact zone.

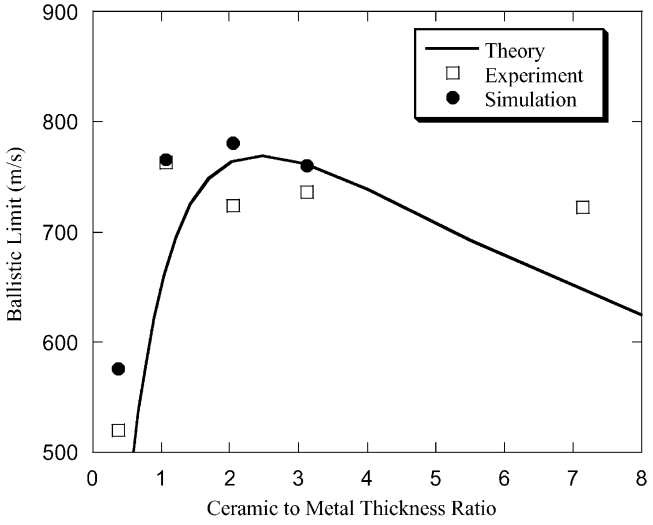

Fig. 11. Ballistic limit velocities for 7.62 AP striking several configurations of equal areal density, 50 kg/m^2. Theoretical and experimental data given by Hetherington [6].

6. Conclusions

The ballistic efficiency of ceramic/metal composite armour systems against 7.62 AP and 40.7 g steel projectiles has been investigated by a combined numerical and experimental approach. The significant phenomena such as, projectile eroding, crack propagation, formation of ceramic conoid and failure of backing plate are well captured by using SPH scheme. Both simulation and experiment reveal the existence of optimum value of the front plate to back plate thickness for a given areal density. The optimum thickness ratio for the configurations considered in the study is shown to be in the region of 2.5. For values of h_1/h_2 between 1.5 and 3, however, ballistic performance of two component composite armours shows no significant difference. It can be concluded that the current simulation method, which is cost-effective than experiment, can be a useful design tool for optimization of lightweight ceramic/metal armour systems. The current simulation can be extended to oblique impact problems.

Acknowledgements

This work was supported by Korea Research Foundation Grant (KRF-99-E00015).

References

[1] Woodward RL. A simple one-dimensional approach to modeling ceramic composite armour defeat. Int J Impact Eng 1990;9(4):455–74.
[2] Zaera R, Sanchez-Galvez V. Analytical modeling of normal and oblique ballistic impact on ceramic/metal lightweight armours. Int J Impact Eng 1998;21(3):133–48.
[3] Wilkins ML. Mechanics of penetration and perforation. Int J Eng Sci. 1978;16:793–807.
[4] Persson A. CM1-A simple model for the dynamic deformation and failure properties of brittle materials. Sweden: Dynamic Research AB, 1990.
[5] Gingold RA, Monaghan JJ. Smoothed particle hydrodynamics: theory and application to non-spherical stars. Mon Not R astr Soc 1997;181:375–89.
[6] Hetherington JG. The optimization of two component composite armours. Int J Impact Eng 1992;12(3):409–14.
[7] Johnson GR, Cook WH. Fracture characteristics of three metals subjected to various strains, strain rates, temperatures and pressures. Eng Fracture Mech 1985;21(1):31–48.
[8] Lee M, Bless S. Cavity models for solid and hollow projectiles. Int J Impact Eng 1998;21(10):881–94.
[9] Wilson D, Hetherington JG. Analysis of ballistic impact on ceramic faced armour using high speed photography. Proceedings Lightweight Armour System Symposium Royal Military Colleage of Science. Cranfield, 1995.